Journal of Fluids Engineering

Technical Briefs

Developing Film Flow on an Inclined Plane With a Critical Point

Kenneth J. Ruschak
Senior Research Associate

Steven J. Weinstein
Research Associate

Manufacturing Research and Engineering Organization, Eastman Kodak Company, Rochester, NY 14652-3701

Kam Ng
Research Associate, Research Laboratories, Eastman Kodak Company, Rochester, NY 14650-2142

Viscous, laminar, gravitationally-driven flow of a thin film on an inclined plane is analyzed for moderate Reynolds number under critical conditions. A previous analysis of film flow utilized a momentum integral approach with a semiparabolic velocity profile to obtain an ordinary differential equation for the film thickness for flow over a round-crested weir, and the singularity associated with the critical point for a subcritical-to-supercritical transition was removable. For developing flow on a plane with a supercritical-to-subcritical transition, however, the same approach leads to a nonremovable singularity. To eliminate the singularity, the film equations are modified for a velocity profile of changing shape. The resulting predictions compare favorably with those from the two-dimensional boundary-layer equation obtained by finite differences and with those from the Navier-Stokes equation obtained by finite elements. [DOI: 10.1115/1.1385516]

Introduction

Laminar flow in thin films at moderate Reynolds number has many practical applications including liquid film coating [1]. Frequently such flows are designed such that film thickness varies gradually in the flow direction. In that case, the classical boundary-layer approximation to the Navier-Stokes equation is justified [2]. However, the boundary-layer equation is still a formidable nonlinear, two-dimensional, partial differential equation that must generally be solved numerically [3].

A standard approach to the boundary-layer equation, attractive for ease of use, is assuming a velocity profile, frequently fixed in shape but variable in magnitude, and minimizing the resulting residual to obtain an ordinary differential equation for the film profile. An inherent drawback is that the initial velocity profile can no longer be arbitrary. Another limitation is the occurrence of a critical point with a singularity, and typically this situation is avoided (for example, [4]) or accommodated (for example, [5]). The film-profile equations are typically first order in the derivative of film thickness when surface tension is neglected [6–8]. The time-dependent film-profile equation, linearized about a steady solution, is hyperbolic and admits wave solutions travelling at the speed of the characteristics [6]. For subcritical flow, waves travel upstream and downstream. For supercritical flow, waves travel downstream only. At a critical point, the coefficient of the derivative of film thickness vanishes. If the rest of the equation can vanish there as well, the singularity may be removable. For developing flow on an inclined plane with a supercritical-to-subcritical transition, the singularity is not removable and the film-profile equation fails, although numerical solutions to the Navier-Stokes and boundary-layer equations can be generated. Similarly, numerical solutions to the boundary-layer equation for decelerating flow on a horizontal plane have been generated [9]. Because the numerical solutions do not require surface tension, it is not key to resolving the breakdown of the film equation and is neglected here. As shown below, the solutions do show that the velocity profile changes shape in the region of the critical point. In light of that observation, the residual approach to the boundary-layer equation is modified here to accommodate a velocity profile of changing shape. The resulting equations for film flow are more complicated but remain tractable. The flow predictions thereby obtained compare favorably to numerical solutions of the boundary-layer and Navier-Stokes equations. With this modification, the residual approach is restored as an option when a velocity profile of fixed shape leads to a critical point with a nonremovable singularity.

Ruyer-Quil and Manneville [10] used a height-averaged approach, and demonstrated that a non-self-similar velocity profile, in which the wall shear stress is different from that predicted from a parabolic velocity profile, yields improved agreement between theoretical and experimental predictions of wave propagation down inclined planes. They obtain additional equations to resolve additional degrees of freedom by evaluating the boundary-layer equation along the boundaries of the film. The approach here is similar, but the focus is on critical flow. The simplest geometry for a transition from supercritical to subcritical flow is considered, and new equations for the film profile are proposed that are not singular. The approach is motivated by numerical solutions to the boundary-layer and Navier-Stokes equations that show a velocity profile of nonconstant shape. Altering the shape of the velocity profile is common in classical boundary-layer flows [2] to improve the accuracy of the predicted wall shear stress and to predict boundary-layer separation; however, the motivation here is avoiding a breakdown of the film-profile equation for a supercritical-to-subcritical transition.

Contributed by the Fluids Engineering Division of THE AMERICAN SOCIETY OF MECHANICAL ENGINEERS. Manuscript received by the Fluids Engineering Division July 28, 2000; revised manuscript received April 16, 2001. Associate Editor: F. K. Wasden.

Experimental Observation

A qualitative experiment was conducted to show a standing wave where laminar flow passes from supercritical to subcritical on a planar, inclined wall. Supercritical flow was distinguished by stationary waves in the wake of a needle touching the surface of the liquid. Subcritical flow was distinguished by periodic flow disturbances, induced by a small, rotating agitator, radiating in all directions. A film in supercritical flow was produced by pumping aqueous glycerol to a distribution die with a slot of height 0.012 cm. The lower half of the die extended from the slot outlet in the flow direction to serve as the inclined plane. Surface tension and surface-tension gradients were reduced by the addition of the surfactant Aerosol® OT (Cytec Industries, Inc.) at high concentration. A small amount of slurry of titanium dioxide was added to the liquid to make it white and opaque. The liquid had a viscosity of 11.8 mPa·s and a specific gravity of 1.11. Lighting by two synchronized strobe lights was adjusted to create shadows revealing the shape of the film. Volumetric flow rate per unit width was fixed at 1.7 cc/s/cm and the inclination of the plane was varied. At sufficiently low angles of inclination, the fully developed flow reached downstream is subcritical. The flow passes from supercritical to subcritical, and the transition is marked by a two-dimensional stationary wave. As inclination increases, the wave moves farther from the slot outlet and becomes less distinct. At sufficiently high angles of inclination, the flow remains supercritical and no wave is apparent. Figure 1 is a photograph showing this evolution for inclinations of 1, 1.5, and 2 degrees.

Equations

A Newtonian liquid with viscosity μ and density ρ flows down a plane inclined at angle θ to horizontal as shown in Fig. 2. The flow evolves from a prescribed initial state and becomes fully developed downstream. Coordinate x increases down the plane, and coordinate y is normal to the plane and outwardly directed. The corresponding velocity components are u and v respectively, and pressure is p. With gravitational acceleration denoted G and volumetric flow rate per unit width q, the film thickness in fully developed, gravitationally driven viscous flow is $h_\infty = [3\mu q/\rho G \sin(\theta)]^{1/3}$. The Reynolds number, $\mathrm{Re}=\rho q/\mu$, significantly exceeds unity so that the length scale along the plane significantly exceeds h_∞.

For gradually varying film thickness, the boundary-layer approximation to the Navier-Stokes equation is justified [7,11,12]:

$$\rho\left[u\frac{\partial u}{\partial x}+v\frac{\partial u}{\partial y}\right]=-\frac{\partial p}{\partial x}+\rho G\sin(\theta)+\mu\frac{\partial^2 u}{\partial y^2} \tag{1}$$

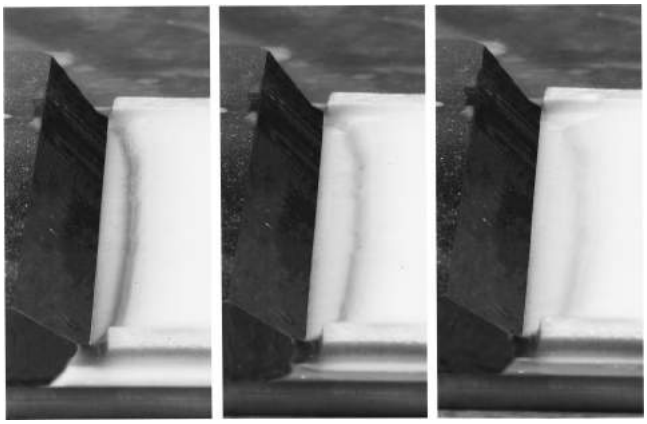

Fig. 1 Photograph showing the standing wave at wall inclinations of 1, 1.5, and 2 degrees. The Reynolds number is 16.

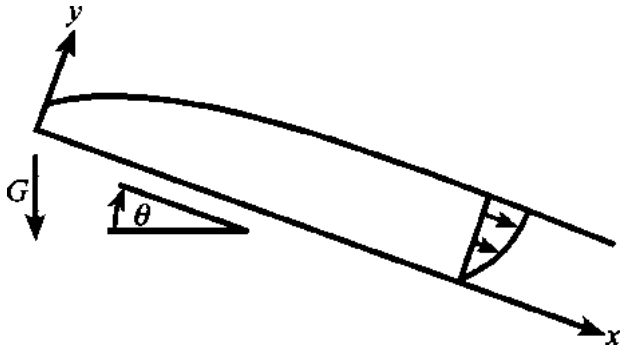

Fig. 2 Definition sketch

$$0=-\frac{\partial p}{\partial y}-\rho G\cos(\theta) \tag{2}$$

The continuity equation is

$$\frac{\partial u}{\partial x}+\frac{\partial v}{\partial y}=0 \tag{3}$$

The surface of the film, $y=h(x)$, is a streamline and free of stress

$$q=\int_0^h u\,dy,\quad \partial u/\partial y=0,\quad p=0\quad (y=h) \tag{4}$$

Velocity is zero at the stationary wall.

$$u=0,\quad v=0\quad (y=0) \tag{5}$$

Finally, the initial film thickness and velocity profile are prescribed.

$$h=h_0,\quad u=u_0(y),\quad (x=0) \tag{6}$$

The following dimensionless variables are introduced:

$$\chi=x/\mathrm{Re}\,h_\infty,\quad H=h/h_\infty,\quad \beta=h_0/h_\infty \tag{7}$$

In applying Eqs. (1)–(6) to film flow, a rectangular domain can be obtained by replacing the coordinate y with y/h. Here, a rectangular domain is obtained through the von Mises transformation [2,12]. In this transformation, the stream function ψ, defined such that $u=\partial\psi/\partial y$ and $v=-\partial\psi/\partial x$, replaces the cross-film coordinate y, and the dependent variable is proportional to the square of the x-component of velocity, $\phi=(uh_\infty/q)^2$. This transformation maps the interface to a fixed boundary location $0\leq\psi\leq q$. With $\Psi=\psi/q$, the resulting nonlinear boundary-value problem for $\phi(\chi,\Psi)$ is:

$$\frac{\partial\phi}{\partial\chi}+\frac{6}{\mathrm{Re}\tan(\theta)}\frac{dH}{d\chi}=\sqrt{\phi}\frac{\partial^2\phi}{\partial\Psi^2}+6 \tag{8}$$

$$\frac{y}{h_\infty}=\int_0^\Psi\frac{dz}{\sqrt{\phi(\chi,z)}},\quad H=\int_0^1\frac{dz}{\sqrt{\phi(\chi,z)}} \tag{9}$$

$$\phi=0\ \ (\Psi=0),\quad \partial\phi/\partial\Psi=0\ \ (\Psi=1) \tag{10}$$

The initial velocity profile ($\chi=0$) is chosen to be either a plug

$$\phi=\beta^{-2} \tag{11}$$

or a half parabola

$$\phi=\beta[1-\cos(\gamma/3)+\sqrt{3}\sin(\gamma/3)],\qquad \gamma=\tan^{-1}[\sqrt{1-(1-\Psi)^2}/(1-\Psi)] \tag{12}$$

For the case of a vertical wall, Eq. (8) becomes that given in [12].

Equations (8)–(10) with either Eq. (11) or (12) were solved by finite differences. It proved necessary to add a second-derivative term to the right-hand side of Eq. (8) of the form $\varepsilon\partial^2\phi/\partial\chi^2$,

where $\varepsilon \ll 1$ is a small number taken to be 10^{-4} in the calculations below. This additional term permits the additional constraint that $H=1$ at the downstream end of the grid $\chi=L$ and thereby suppresses a solution describing a horizontal interface in which the derivative of film thickness on the left-hand side of Eq. (8) balances the constant on the right-hand side.

To implement finite differences, new variables χ' and Ψ' are defined that permit more mesh points to be located near $\chi=0$ and $\Psi=0$, namely, $\chi'=[\log(\chi+\delta_\chi)-\log(\delta_\chi)]/[\log(L+\delta_\chi)-\log(\delta_\chi)]$ and $\Psi'=[\log(\Psi+\delta_\Psi)-\log(\delta_\Psi)]/[\log(1+\delta_\Psi)-\log(\delta_\Psi)]$, where δ_χ and δ_Ψ are constants. In the calculations, $\delta_\chi=10^{-6}$ and $\delta_\Psi=10^{-2}$, and the numbers of uniform segments in the χ' and Ψ' directions were 100 and 50, respectively. The solution was obtained iteratively in MATLAB by Newton's method. For most cases, a solution of Eq. (8) without the term in $dH/d\chi$, obtained as previously described [3], provided an initial guess. As $\mathrm{Re}\tan(\theta)$ was set to smaller values, the previously converged solution supplied an initial guess. In addition to numerical solutions of the boundary-layer equation, solutions of the Navier-Stokes equation were generated by the finite element method [3].

An approach simpler than the Von Mises transformation is to assume a velocity profile and to integrate Eq. (1) across the film. The partial differential equation thereby reduces to an ordinary differential equation. A frequent assumption is that the velocity profiles at all cross sections are geometrically similar, and a common choice for the shape is a half parabola. For the problem at hand, however, a geometrically similar profile fails if there is a critical point, and to avoid this outcome a more general velocity profile is employed. With $\eta=y/h$,

$$uh/q=A[\eta-5\eta^2/2+4\eta^3/3]+3[\eta-\eta^2/2] \quad (0\leqslant\eta\leqslant 1) \tag{13}$$

The function $A(x)$ alters the shape of the velocity profile and is determined as part of the solution. This profile is a cubic polynomial that reduces to a half parabola for $A=0$, and in the present problem A asymptotes to zero downstream. Eq. (13) is consistent with Eqs. (4) and (5). Velocity component v follows from Eqs. (13), (3), and (5), and pressure follows from Eqs. (2) and (4).

$$p=\rho G\cos(\theta)(h-y) \tag{14}$$

Equation (1), evaluated from these expressions for u, v, and p, leaves residual R. The two equations required to solve for H and A are generated by requiring the average of the residual to be zero over two intervals.

$$\frac{1}{\omega}\int_0^\omega R\,d\eta=0 \tag{15}$$

The extent of an interval is specified by ω, $0<\omega\leqslant 1$. The choice $\omega=1$ gives an overall momentum balance.

$$\left[\frac{3}{\mathrm{Re}\tan(\theta)}-\frac{\alpha}{H^3}\right]\frac{dH}{d\chi}+\frac{1}{H^2}\frac{d\alpha}{d\chi}=3-\frac{3+A}{H^3} \tag{16}$$

$$\alpha=6/5-A/15+A^2/105 \tag{17}$$

Computational experiments were carried out over the range of second values for ω. The outcome, summarized below, leads to the limit of Eq. (15) as $\omega\to 0$ with the result $R=0$ at $\eta=0$.

$$0=-1+\frac{1}{\mathrm{Re}\tan(\theta)}\frac{dH}{d\chi}+\frac{5A/3+1}{H^3} \tag{18}$$

Eqs. (16) and (18) can be rearranged as

$$-\alpha\frac{dH}{d\chi}+H\frac{d\alpha}{d\chi}=4A \tag{19}$$

$$\frac{dH}{d\chi}=\mathrm{Re}\tan(\theta)\left[1-\frac{5A/3+1}{H^3}\right] \tag{20}$$

A solution to Eqs. (19) and (20) is sought for H and A that asymptotes to fully developed flow downstream, $A\to 0(\chi\to\infty)$ and from Eq. (20) $H\to 1(\chi\to\infty)$. A numerical integration is started from an asymptotic solution obtained by linearizing Eqs. (19) and (20) about fully developed flow. The asymptotic solution comprises terms in $e^{m\chi}$ where m is the root of a quadratic equation. For θ positive and less than 90 deg, there is one positive and one negative real root, and the negative root is selected so that the departure from fully developed flow decays downstream.

For a velocity profile that is geometrically similar at each cross section, A is a constant and Eq. (16), the overall momentum balance, reduces to

$$\left[\frac{3}{\mathrm{Re}\tan(\theta)}-\frac{\alpha}{H^3}\right]\frac{dH}{d\chi}=3-\frac{3+A}{H^3} \tag{21}$$

The coefficient of $dH/d\chi$ in this equation determines whether flow is subcritical (coefficient positive) or supercritical (coefficient negative) according to wave propagation [6]. The fully developed flow is critical whenever $\mathrm{Re}\tan(\theta)=3/\alpha$. For flow that is everywhere supercritical, Eq. (21) admits a solution that tends to fully developed flow. On the other hand, if the flow is everywhere subcritical, or if the flow passes from supercritical to subcritical, there is no solution to Eq. (21) tending to fully developed flow. Moreover, the singularity at the critical point cannot be removed by requiring that the right-hand-side of Eq. (21) vanish at the critical point. Therefore, a velocity profile of fixed shape fails in the problem at hand.

Results

When the initial film thickness is much less than that far downstream ($H\ll 1$), gravitational effects are initially negligible and the solution is a well known similarity solution for which film thickness grows linearly [3]. This similarity solution is a Jeffery-Hamel flow, an exact solution of the Navier-Stokes equation for radially diverging streamlines [13]. Equations (16)–(18) admit such a solution, specifically $A=-3/5$, $\alpha=1088/875$, and $dH/d\chi=525/272$, if the terms arising from gravity are dropped or, equivalently, if just the leading terms are retained as $H\to 0$. Choices for ω in Eq. (15) other than $\omega\to 0$ do not produce this limiting case and so are less useful. Figure 3 illustrates this outcome for $\mathrm{Re}=50$ and $\theta=3$ deg. Different nonzero values for ω yield similarly shaped but truncated solution curves that abruptly

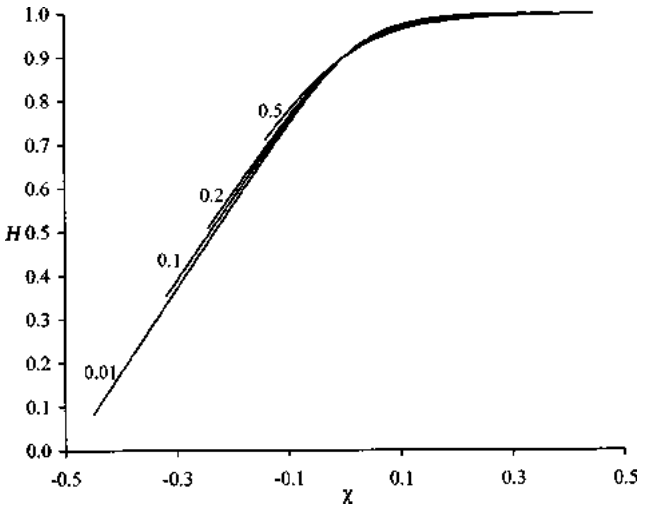

Fig. 3 Film profiles for Re=50 and θ=3 deg at four values of ω in Eq. (15). The profiles terminate abruptly because of a zero determinant.

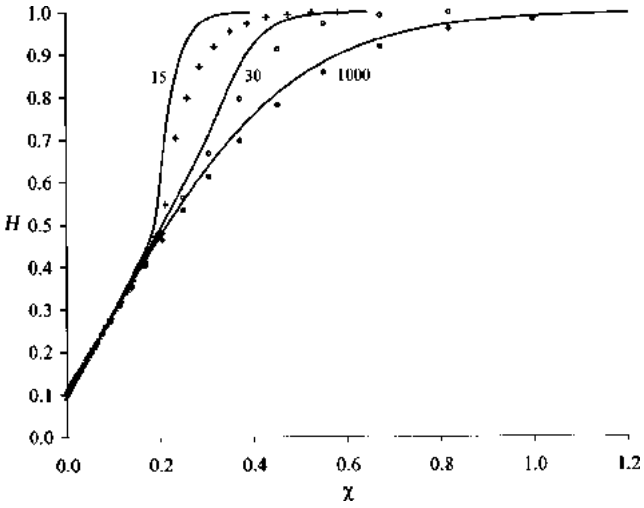

Fig. 4 Film profiles for three values of Re at θ=3 deg from Eqs. (19) and (20) (solid lines) and from the boundary-layer equation (points)

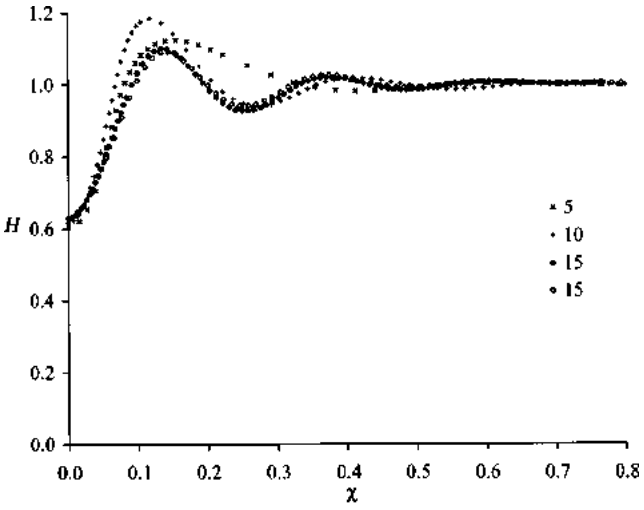

Fig. 5 Film profiles by the finite element method for three values of Re at θ=3 deg. Results for two meshes at Re=15 support a conclusion that the waves are not a numerical artifact.

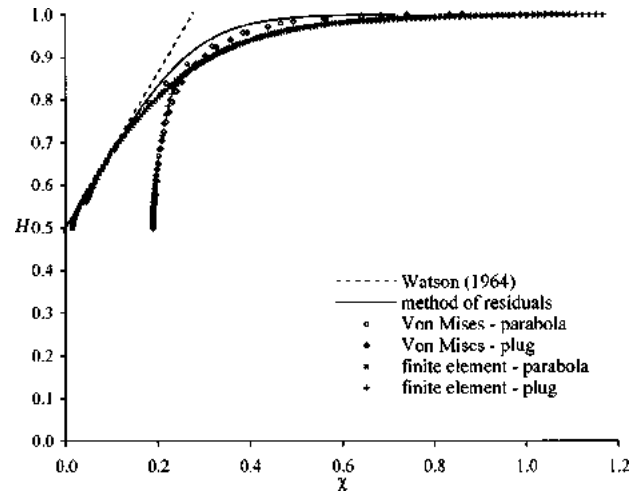

Fig. 6 Film profiles for Re=50 and θ=3 deg from the solution of the boundary layer equation by the method of residuals, from the solution of the boundary layer equation by the Von Mises transformation, and from the solution of the Navier-Stokes equation by the finite-element method. Also shown is the linear profile for negligible gravity [14].

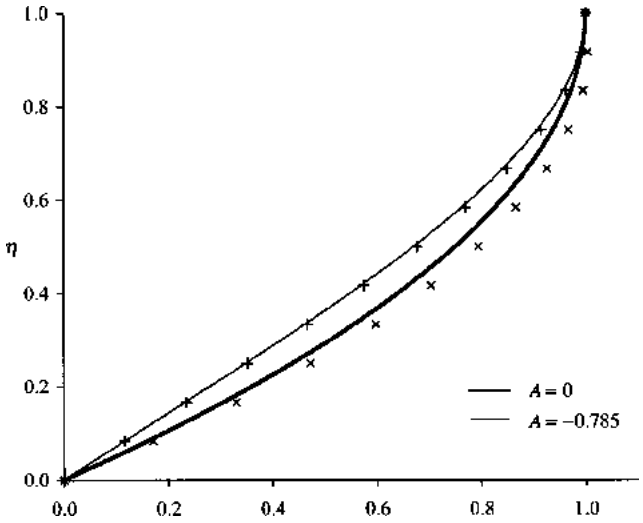

Fig. 7 Extreme velocity profiles for Re=30 and θ=3 deg from the method of residuals (solid curves) and from the finite element method (points)

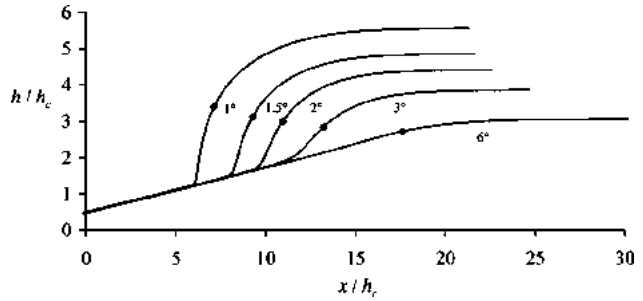

Fig. 8 Film profiles at five angles of inclination for the conditions of the photo. The circles show the location where the coefficient of $dH/d\chi$ in Eq. (16) vanishes.

end where the determinant of the equations becomes zero. Consequently, all of the following results are for the choices ω=1 and $\omega \rightarrow 0$ in Eq. (15).

Equations (19) and (20) admit a solution at Reynolds numbers of order unity and greater as shown in Fig. 4 for θ=3 deg. Also shown in Fig. 4 are solutions of the boundary layer equation by the Von Mises transformation with an initial parabolic velocity profile. The agreement improves as Re increases. The dimensionless profile does not change for values of Re exceeding 1000. At Reynolds numbers of order unity, the small-slope assumption breaks down, and solutions to the Navier-Stokes equation by the finite-element method produce film profiles that oscillate spatially as shown in Fig. 5. The boundary-layer equations do not capture these standing waves.

A more detailed comparison for Re=50 and θ=3 deg is shown in Fig. 6. The linear profile for negligible gravitational effects [14] is shown and is closely approached by the profile from the method of residuals, Eqs. (19) and (20). Solutions of the Navier-Stokes equation by the finite element method and of the boundary-layer equation by the Von Mises transformation for the cases of initial plug and parabolic velocity profiles are also shown and are nearly indistinguishable. The film profile in the parabolic case quickly approaches the Jeffery-Hamel similarity solution, but that in the plug case approaches fully developed flow directly. The method of residuals cannot capture differences arising from initial velocity profiles.

Velocity profiles according to the method of residuals are com-

pared with those from the finite element method in Fig. 7 for $\mathrm{Re}=30$ and $\theta=3$ deg. Velocity profiles for the extreme values of A, 0 and -0.785, are plotted as smooth curves. The extreme profiles from the finite-element method are plotted as points. The method of residuals captures the range of velocity profiles reasonably well, and this agreement supports the conclusion that a velocity profile of fixed shape is unworkable in the present problem.

Figure 8 shows film profiles by the method of residuals at $\mathrm{Re}=16$, the value for the conditions of the experimental observation. In accordance with Fig. 1, the profiles show a prominent standing wave that shifts downstream and fades as the inclination of the plane increases.

Concluding Remarks

Although the shape of the velocity profile changes in the transition from supercritical to subcritical flow, the change is modest according to Fig. 7. Nonetheless, any inference that a half parabola should suffice for the velocity profile is incorrect. There is a region in the flow where the dominant terms in Eqs. (19) and (20) nearly cancel. The small difference is offset by the term related to the changing shape of the profile, the term in $d\alpha/d\chi$. This term precludes a singular solution and provides access to fully developed flow downstream.

The cubic velocity profile approximates Jeffery-Hamel flow more accurately than a parabolic velocity profile. The slope of the linear film profile determined above, 1.93, is near the expected value, 1.81 [14]. On the other hand, a parabolic velocity profile gives 2.5 [3]. A cubic profile, unlike a parabolic profile, can accommodate the inflection point at the wall inherent in the Jeffrey-Hamel solution.

The choice $\omega\rightarrow 0$ in Eq. (15) is equivalent to evaluating the Navier-Stokes equation at the wall, a common step in classical boundary-layer analysis. The inertial terms vanish at the wall, and it is that outcome that precludes a vanishing determinant. So, our findings support the classical approach to providing an additional equation.

Flow is everywhere supercritical in the case of a vertical plane, and consequently the many analyses of that special case have not encountered a critical point.

The evident success of the present approach suggests that it be generalized to more complicated flows and explored more extensively. Such work is in progress.

Acknowledgment

The photograph was taken by Paul DeVries of Eastman Kodak Company.

References

[1] Kistler, S. F., and Schweizer, P. M., eds., 1997, *Liquid Film Coating*, Chapman & Hall, New York.
[2] Schlichting, H., 1979, *Boundary-Layer Theory*, 7th edition, McGraw-Hill, New York, pp. 157–158.
[3] Ruschak, K. J., and Weinstein, S. J., 2000, ''Thin-Film Flow at Moderate Reynolds Number,'' ASME J. Fluids Eng., **122**, pp. 774–778.
[4] Alekseenko, S. V., Nakoryakov, V. E., and Pokusaev, B. G., 1994, *Wave Flow of Liquid Films*, Begell House, Inc., New York.
[5] Thomas, S., Hankey, W., and Faghri, A., 1990 ''One-Dimensional Analysis of the Hydrodynamic and Thermal Characteristics of Thin Film Flows Including the Hydraulic Jump and Rotation,'' ASME J. Heat Transfer, **112**, pp. 728–735.
[6] Ruschak, K. J., and Weinstein, S. J., 1999, ''Viscous Thin-Film Flow Over a Round-Crested Weir,'' ASME J. Fluids Eng., **121**, pp. 673–677.
[7] Anderson, H. I., 1984, ''On Integral Method Predictions of Laminar Film Flow,'' Chem. Eng. Sci., **39**, pp. 1005–1010.
[8] Anderson, H. I., 1987, ''The Momentum Integral Approach to Laminar Thin-Film Flow,'' Proc. ASME Symposium on Thin Films, Vol. **48**, pp. 7–13.
[9] Higuera, F. J., 1994, ''The hydraulic jump in viscous laminar flow,'' J. Fluid Mech., **274**, pp. 69–92.
[10] Ruyer-Quil, C., and Manneville, P., 1998, ''Modeling film flows down inclined planes,'' The European Physical Journal B, **6**, pp. 277–292.
[11] Bruley, D. F., 1965, ''Predicting Vertical Film Flow Characteristics in the Entrance Region,'' AIChE J., **11**, 945–950.
[12] Cerro, R. L., and Whitaker, S., 1971, ''Entrance Region Flows With a Free Surface: the Falling Liquid Film,'' Chem. Eng. Sci., **26**, pp. 785–798.
[13] Rosenhead, L., 1940, ''The Steady Two-Dimensional Radial Flow of Viscous Fluid Between Two Inclined Plane Walls,'' Proc. R. Soc. London, Ser. A, **175**, pp. 436–467.
[14] Watson, E. J., 1964, ''The Radial Spread of a Liquid Jet Over a Horizontal Plane,'' J. Fluid Mech., **20**, pp. 481–499.

